Supplementary Information

Inexpensive gram scale synthesis of porous Ti_4O_7 for high performance polymer electrolyte fuel cell electrodes

Mitsuharu Chisaka[*a] *Waka Nagano,*[*b] *Byambasuren Delgertsetseg,*[*b] *and Tatsuya Takeguchi*[*b]

[a]Department of Sustainable Energy, Hirosaki University,

3 Bunkyo-cho, Hirosaki, Aomori 036-8561, Japan

[b]Faculty of Science and Engineering, Iwate University,

4-3-5 Ueda, Morioka, Iwate 020-8551, Japan

*Authors to whom correspondence should be addressed.

Phone/Fax: +81 172 39 3559; E-mail: chisaka@hirosaki-u.ac.jp (M. Chisaka)

Phone: +81 196 21 6329; Fax: +81 196 21 6335; E-mail: wnagano@iwate-u.ac.jp (W. Nagano)

Phone: +81 196 21 6329; Fax: +81 196 21 6335; E-mail: delgerts@iwate-u.ac.jp (B. Delgertsetseg)

Phone/Fax: +81 196 21 6335; E-mail: takeguch@iwate-u.ac.jp (T. Takeguchi)

S1. Experimental details.

The Ti_4O_7 supports were synthesized via a carbothermal reduction route[S1] with some modifications and then platinum nanoparticles were supported on Ti_4O_7 by using a recently reported ethanol reduction method.[S2] The obtained Pt/Ti_4O_7 catalysts were characterized to reveal the physical/chemical properties and electrochemical performance in both a half cell and a single cell.

S1-1. Synthesis of Ti_4O_7 supports.

The Nazar group reported carbothermally reduced Ti_4O_7 particles for lithium-sulfur battery cathodes.[S1] In this study, their synthesis route was modified by using: (1) a combination of titanium oxysulfate/water precursor/dispersant instead of titanium ethoxide/ethanol; (2) higher drying temperatures; and (3) different annealing conditions. Moreover, the mass fraction of titanium in the precursor dispersion, which was not described in the reference S1, was optimized to obtain the Ti_4O_7 phase. As titanium oxysulfate is stable to the moisture in air and therefore easy to handle, we selected it as a titanium precursor as it is more suitable for the mass production of Ti_4O_7 compared with titanium ethoxide or other titanium sources that react readily with moisture in the air. In addition, water was used instead of ethanol[S1] to reduce the cost of synthesis. Based on this precursor modification (1), other modifications (2) and (3) were performed, and the results are shown later in section S3. First, 24.5 g of titanium oxysulfate ($TiOSO_4 \cdot nH_2O$; $n \approx 1–2$, Kishida Chemical Co. Ltd., Osaka, Osaka, Japan) was dispersed in a mixture of distilled water and polyethylene glycol ($H(OCH_2CH_2)_nOH$, the average molecular weight was between 360 and 440, hereafter denoted as PEG400; Fuji Film Wako Pure Chemical Co., Osaka, Osaka, Japan) by magnetic stirring at room temperature in a glass beaker. The mass ratio of PEG400 to $TiOSO_4$-derived TiO_2 was set constant at 1, unless otherwise noted, and the volume of the water-PEG400 mixture was adjusted to 500 cm^3 at any mass ratio. The glass beaker was set in an aluminum bath filled with aluminum beads, stirred continuously, and heated to 353 K overnight. The dispersion was white at room temperature, but upon heating, a yellow solution was formed; then, after heating at 353 K overnight, the solution turned to a brown gel. This gel was

transferred to an alumina boat and the boat was then placed in an open-end quartz tube furnace and dried at 423 K. As an alternative method, the gel could be continuously dried at 423 K in the aluminum bead-filled aluminum bath. With either method, the brown gel was transferred into a black powder, regardless of the drying apparatus. Third, the black powders were ground using an agate mortar, transferred to another alumina boat, and sealed tightly in a quartz tube furnace. The first to third steps, i.e., mixing of precursors to sealing the black powders in the quartz tube furnace, were performed in a fume hood. Then the tube furnace was removed from the hood. After the tube was purged with N_2 gas for more than 20 min, the flowing gas was changed to 10% v/v H_2/Ar, and the powder samples were heated from room temperature to various temperatures between 1173 K and 1273 K at a rate of 10 K min^{-1}, then maintained at that temperature for 3 h. The samples were then cooled to room temperature at an uncontrolled rate to allow annealing. After annealing, the powders were ground in an agate mortar. For comparison, titanium tetrafluoride (TiF_4, Sigma-Aldrich Co., St. Louis, Missouri, USA) was used instead of titanium oxysulfate; in this case, a polytetrafluoroethylene (PTFE) beaker was used instead of a glass beaker.

The reference Ti_4O_7 powders were synthesized by simple annealing. First, 0.4 g of a commercial TiO_2 powder (ST-01, Ishihara Sangyo Co., Osaka, Osaka, Japan) was placed in an alumina boat and the boat was placed in a quartz tube furnace and evacuated for more than 10 min. The tube was then purged with 10% v/v H_2/Ar, heated to 1323 K at a rate of 10 K min^{-1}, held at 1323 K for 6 h, and then cooled at an uncontrolled rate. The size of reference large Ti_4O_7 powders exceeded 1 μm (Fig. 1(b)); the powder is henceforth referred to as Ti_4O_7-L.

S1-2. Synthesis of Pt/Ti_4O_7 and Pt/SnO_2 catalysts

First, diamminedinitritoplatinum(II) solution ($Pt(NO_2)_2(NH_3)_2$, Tanaka Kikinzoku Kogyo Co. Ltd., Chiyoda-ku, Tokyo, Japan) and 0.6 g of Ti_4O_7 or Ti_4O_7-L supports were dispersed in 200 cm^3 of distilled water by magnetic stirring at room temperature for 1 h. The amount of $Pt(NO_2)_2(NH_3)_2$ was varied to obtain various platinum-loaded catalysts with 5%–30% w/w Pt/(Pt +Ti_4O_7). Then, 30 cm^3 of

ethanol was added and stirred continuously at room temperature for 30 min. The temperature was increased to 368 K and maintained for 12 h with continuous stirring. The catalysts were then vacuum filtered, washed with 1 dm^3 of distilled water, and dried at room temperature for 12 h. Finally, the catalysts were dried using a two-step process in a quartz tube furnace: 1) 353 K for 10 h under N_2 gas flow; 2) 473 K for 2 h under He gas flow. For reference, 20% w/w Pt/SnO_2 catalyst was synthesized under the identical conditions except for using SnO_2 particles (22–43 nm, Fuji Film Wako Pure Chemical Co., Osaka, Osaka, Japan) as supports instead of Ti_4O_7.

S1-3. Characterization

The morphology of the catalysts was investigated using a field emission scanning electron microscope and a transmission electron microscope (JSM-7000F and JEM-2100, respectively, JEOL, Akishima, Tokyo, Japan). The bulk crystal structures of catalysts were analyzed using an X-ray diffractometer (MiniFlex600, Rigaku Co., Akishima, Tokyo, Japan) with Cu-Kα radiation generated at 40 kV and 15 mA (scan range = 20°–80°, step size = 0.02°, and scan rate = 2° min^{-1}). The surface crystal structures were evaluated using a Raman spectrometer (NRS-5100, JASCO Co. Ltd., Hachioji, Tokyo, Japan) with a 532-nm laser. The chemical states of the catalysts were determined using an X-ray photoelectron (XP) spectrometer (PHI 5000 VersaProbe, ULVAC-PHI, Inc., Chigasaki, Kanagawa, Japan) with an Al-Kα X-ray source (1486.6 eV). The peak shifts due to the surface charge were corrected using the binding energy of C 1s (284.8 eV) from the organic contaminants in the spectrometer or air. As three components –contaminants, surface titanium oxide layers, and platinum oxide layers– could contribute to the O 1s spectra of the catalysts in a manner that prevented them from being distinguished from each other, the Ti 2p and Pt 4f spectra were analyzed in this study. Nitrogen adsorption isotherms were measured by using a surface area and pore size distribution analyzer (BELSORP MINI X, MicrotracBEL Co., Osaka, Osaka, Japan) at 77 K. The conductivity, σ, of the support materials and commercial carbon black (Ketjen black EC600JD, Lion Co., Sumida-

ku, Tokyo, Japan) was measured by a four-probe method at compression pressures, P, ranging from 3 to 64 MPa using a powder resistivity measurement system (MCP-PD600, Nittoseiko Analytech Co., Yamato, Kanagawa, Japan). Both platinum particle size, d_{Pt}, and chemically active area of platinum particles, S_{CSA}, were measured with a carbon monoxide (CO) pulse method using a catalyst analyzer (BELCAT II, MicrotracBEL Co., Osaka, Osaka, Japan). Particle size of Ti_4O_7 supports was measured using a nano particle analyzer (nano partica SZ-100V2, Horiba Ltd.). The compositions of the Pt/Ti_4O_7 catalysts were evaluated using an X-ray Fluorescence (XRF) spectrometer (S8 TIGER, Bruker AXS Inc., Madison, WI, USA) and a Thermogravimeter-Differential Thermal Analyzer (TG/DTA7200, Seiko Instrument Inc., Chiba, Chiba, Japan).

S1-4. Electrochemical characterization

CO stripping voltammetry in a conventional three-electrode cell was used to evaluate the electrochemically active surface area, S_{ECSA}, of the Pt/Ti_4O_7 catalysts. First, a glassy carbon (GC) disk electrode with a diameter of 5 mm (Pine Research Instrumentation, Durham, North Carolina, U.S.) was polished with an alumina slurry (0.05 μm, Buehler Co., Minato-ku, Tokyo, Japan), cleaned by sonication in ethanol for 10 min, and then sonicated in deionized water for 10 min. The GC electrode was then dried thoroughly before coating with the catalyst layers. Subsequently, the catalyst inks were prepared by sonicating the Pt/Ti_4O_7 catalyst, 2 cm^3 of deionized water, 3 cm^3 of ethanol, and 0.05 cm^3 of 5% w/w Nafion solution (Sigma-Aldrich Co., St. Louis, Missouri, U.S.) for 15 min. Third, 0.01 cm^3 of catalyst ink was uniformly spread on the polished GC electrode, the solvent was evaporated in air, and then the electrode was placed in an oven at 373 K for 15 min. The platinum loading on the GC disk electrode was kept at 17.6 $\mu g_{Pt}\ cm^{-2}$ by controlling the mass of the Pt/Ti_4O_7 catalyst with various platinum fractions, w_{Pt}, in the catalyst ink. A three-electrode cell filled with 0.1 mol dm^{-3} $HClO_4$ was placed in a water bath at 298 K. The catalyst-coated GC disk electrode, a platinum coil, and an Ag/AgCl (sat. KCl) electrode were used as the working, counter, and reference electrodes, respectively. The working electrode was set on a rotator (AFMSRCE, Pine Research Instrumentation, Durham, North

Carolina, U.S.) connected to a PARSTAT MC multichannel potentiostat (AMETEK Scientific Instruments, Zoeterwoude, The Netherlands). All working electrode potentials were in relation to the reversible hydrogen electrode (RHE). After the electrolyte solution was bubbled with Ar for 15 min, the platinum surface was cleaned by scanning the potential between 0.05 V and 1.20 V at 50 mV s^{-1}. The baseline cyclic voltammograms (CVs) were then measured between 0.05 and 1.10 V at a scan rate of 5 mV s^{-1}. Subsequently, the electrolyte was bubbled with CO, keeping the potential at 0.05 V for 15 min to cover all the exposed platinum surface with CO. The electrolyte was purged with Ar for 15 min to eliminate dissolved CO in the electrolyte and the CVs were then measured as described above. The CVs obtained through this process is called a CO stripping voltammogram because the CO molecules adsorbed on platinum surface were electrochemically oxidized as follows:

$$Pt–CO + H_2O \rightarrow Pt + CO_2 + 2H^+ + 2e^- \quad \text{(S1)}$$

which gives rise to a peak at approximately 0.8 V, as shown in Fig. S1.

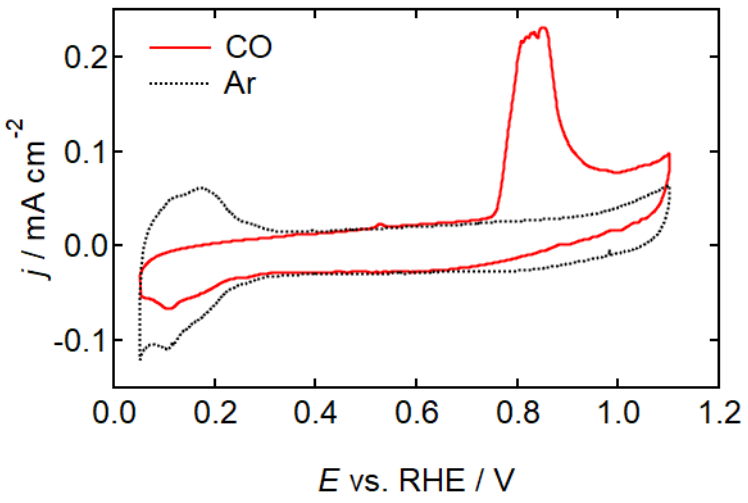

Fig. S1. A CO stripping voltammogram and the baseline cyclic voltammogram of 20% w/w Pt/Ti_4O_7. The scans were performed under CO and Ar atmospheres at a scan rate of 5 mV s^{-1} in 0.1 mol dm^{-3} $HClO_4$. The platinum loading was 0.0176 mg_{Pt} cm^{-2}.

The S_{ECSA} of the Pt/Ti_4O_7 catalysts was evaluated from the charge associated with the electrochemical oxidation of CO (eq. S1), Q_{CO}, by using equation S2:

$$S_{ECSA} = Q_{CO}/(L_{Pt} \times 0.420 \text{ mC cm}^{-2}) \quad \text{(S2)}$$

where Q_{CO} (mC) is the electrochemical charge for the CO oxidation, L_{Pt} (g) is the amount of Pt on the GC electrode, and 0.420 (mC cm^{-2}) is the charge required for the oxidation of CO monolayer per unit area of flat platinum surface.[S3]

S1-5. Single cell tests

Gas diffusion layers (GDLs) were prepared by painting microporous layers on carbon paper with a thickness of 0.17 mm (P50T, AvCarb Material Solutions, Lowell, Massachusetts, USA).[S2] The catalyst inks for membrane electrode assemblies (MEAs) were prepared by sonicating Pt/Ti_4O_7, commercial Pt/C (TEC10E50E, Tanaka Kikinzoku Kogyo Co. Ltd**.,** Chiyoda-ku, Tokyo, Japan), or Pt/Ti_4O_7-L catalyst with 5% w/w Nafion solution and ethanol for 15 min. The mass ratio of Pt/Ti_4O_7 or Pt/C or Pt/Ti_4O_7-L catalyst:Nafion was set at 9:1. The obtained inks were uniformly painted on the home-made GDL to obtain gas diffusion electrodes (GDEs) and the catalyst layer area was 2.2 × 2.2 cm^2. The GDEs were dried overnight and MEAs were prepared by hot-pressing the anode and cathode GDEs onto both sides of a membrane (NRE-212, Sigma-Aldrich Co., St. Louis, Missouri, U.S.) at 10.0 MPa and 408 K for 20 min. Single cells were fabricated by assembling the MEAs with graphite plates with straight flow fields shielded with silicon robber gaskets. All tests were performed at 353 K without applying back pressure. The reactant gases, H_2 and O_2, were humidified by passing through separate water baths at 353 K for H_2 and 348 K for O_2. Both gas flow rates were 85 cm^3 per min and the current density−voltage (i−V) curves were measured galvanostatically using the Solartron 1280Z electrochemical test system (AMETEK Scientific Instruments, Zoeterwoude, The Netherlands). Accelerated degradation tests (ADTs) were performed using a protocol proposed at the Fuel Cell Commercialization Conference of Japan (FCCJ).[S4]

S2. Mass fraction of platinum in Pt/Ti_4O_7 catalysts.

Pt/Ti_4O_7 catalysts with four different w_{Pt} of 5, 10, 20 and 30% w/w were synthesized by putting different mass of $Pt(NO_2)_2(NH_3)_2$ into a precursor dispersion. The w_{Pt} value of the catalysts evaluated using an XRF spectroscopy, $w_{Pt,\,XRF}$, is plotted as a function of the nominal mass fraction of platinum calculated from the mass of $Pt(NO_2)_2(NH_3)_2$ and Ti_4O_7 used for the synthesis, w_{Pt}, in Fig. S2. The $w_{Pt,\,XRF}$ is almost the same as w_{Pt} and the standard deviations displayed by error bars are small enough when $w_{Pt} \leq 20\%$ w/w, indicating that the precursors were mixed well and did not evaporate during the annealing. A large error bar is observed at $w_{Pt} = 30\%$ w/w, suggesting that some improvements are needed to prepare the precursors. Overall, it is fair to say that the w_{Pt} of Pt/Ti_4O_7 is well controlled by simply changing the mass of $Pt(NO_2)_2(NH_3)_2$ in the precursor dispersion.

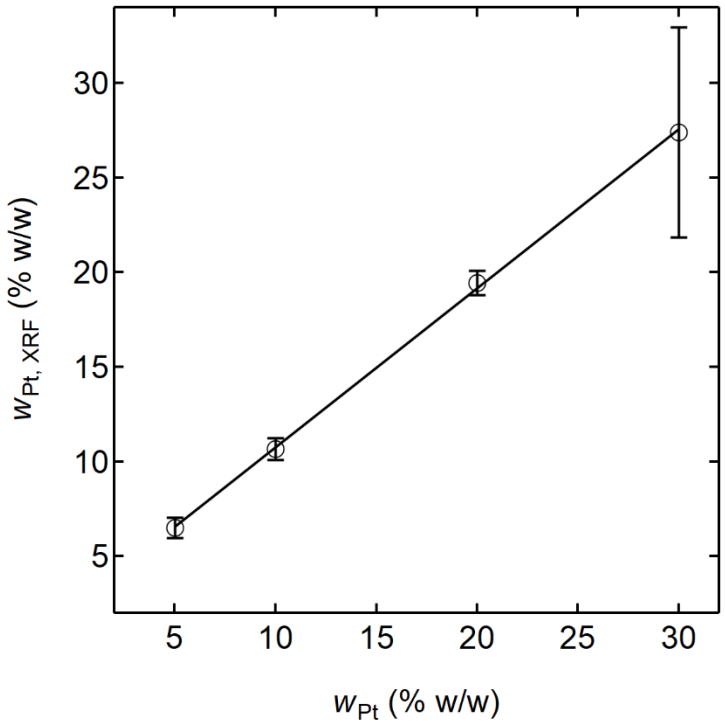

Fig. S2 Mass fraction of platinum measured using an X-ray Fluorescence spectroscopy versus that calculated from the mass of $Pt(NO_2)_2(NH_3)_2$ and Ti_4O_7 precursors ($w_{Pt,\,XRF}$ – w_{Pt} curve of Pt/Ti_4O_7 catalysts).

S3. Effect of synthesis conditions on the crystal structure of supports.

The bulk and surface crystal structure of the supports was evaluated using XRD and Raman spectroscopy, respectively. Although Nazar group reported that they dried the precursor mixture from titanium ethoxide and PEG400 at 373 K then annealed at 1223 K to obtain Ti_4O_7 particles, we dried present precursor mixture from titanium oxysulfate and PEG400 at a higher temperature, 423 K, as sulfurous species from titanium oxysulfate remained even after the high-temperature annealing when the drying temperature was 373 K; the resulting sample after the annealing at 1223 K smelled notably sulfurous and analyses were impossible. The XRD pattern of the support annealed at temperature, T = 1173 K displayed a Ti_9O_{17} phase, as shown in Fig. S3(A), whereas a mixture of Ti_8O_{15} and Ti_7O_{13} phases appeared when T was increased to 1210 K, as shown in Fig. S3(B). Moreover, these two supports displayed a small peak at around 25.2º, which may have originated from the (0 0 2) plane of the graphitic carbon from the PEG400 precursor. The peak at approximately 25.2º was significantly smaller when T was increased to 1240 K, indicating a single Ti_4O_7 phase as shown in Fig. S3(C). When the temperature was increased to 1273 K, the suboxide was further reduced to display a single Ti_3O_5 phase as shown in Fig. S3(D). When the mass ratio of PEG400 to $TiOSO_4$-derived TiO_2 was reduced to 0.5, the samples were oxidized, e.g., a mixture of Ti_4O_7 and Ti_5O_9 phases was obtained at T = 1240 K, in contrast to a single Ti_4O_7 phase that was observed when the mass ratio was doubled (Fig. S3(C)). These results indicate that the carbon species from the PEG400 precursor produced a reductive atmosphere to proceed carbothermal reduction reaction, i.e., the oxygen atoms in the titanium oxide lattice were removed by reaction with the PEG400-derived carbon species. Therefore, the number of oxygen atoms per unit titanium atom decreased at higher T, as shown from the XRD analysis. The XRD patterns shown in Fig. S3 indicate that the composition can be easily controlled by T. An even more reduced phase can be obtained by reducing the number of oxygen atoms from the titanium precursor: when titanium tetrafluoride was used instead of titanium oxysulfate, a single Ti_2O_3 phase was obtained, as shown in Fig. S4. The electric conductivity of Magnéli phase titanium oxide is known to depend on the composition and the highest conductivity is obtained from a Ti_4O_7 phase.[S5] The mass of the Ti_4O_7 particles was easily

increased by simply increasing the mass of precursor powders in the furnace, as shown in Fig. S5. After annealing at 1240 K, approximately 2 g of Ti_4O_7 particles was successfully obtained in a single reaction without increasing the annealing duration. Thus, the present simple synthesis route enabled gram-scale production of Ti_4O_7 with a low-cost titanium source, titanium oxysulfate, which can be handled in air.

A Raman spectrum of the Ti_4O_7 particles is shown in Fig. S6. Two sharp peaks are displayed, at approximately 417 and 602 cm^{-1}, and were assigned to the E_g and A_{1g} vibration modes of rutile TiO_2, respectively.[S6,S7] A broader peak observed at approximately 250 cm^{-1} was assigned to second-order scattering or disorder of TiO_6 octahedra.[S6] Given the deeper penetration into the bulk sample obtained by XRD than Raman spectroscopy,[S8] the results from Fig. S3(C) and Fig. S6 indicate that the surface of Ti_4O_7 was oxidized to form rutile TiO_2 layers. Compared with the Raman spectrum of commercial rutile TiO_2 powders, only the E_g peak was significantly shifted to a lower wavenumber, indicating that many oxygen vacancies were incorporated into the surface rutile TiO_2 layers.[S8] Oxygen vacancies in rutile TiO_2 favor the dissociative adsorption of oxygen molecules,[S9] the first step of the oxygen reduction reaction.

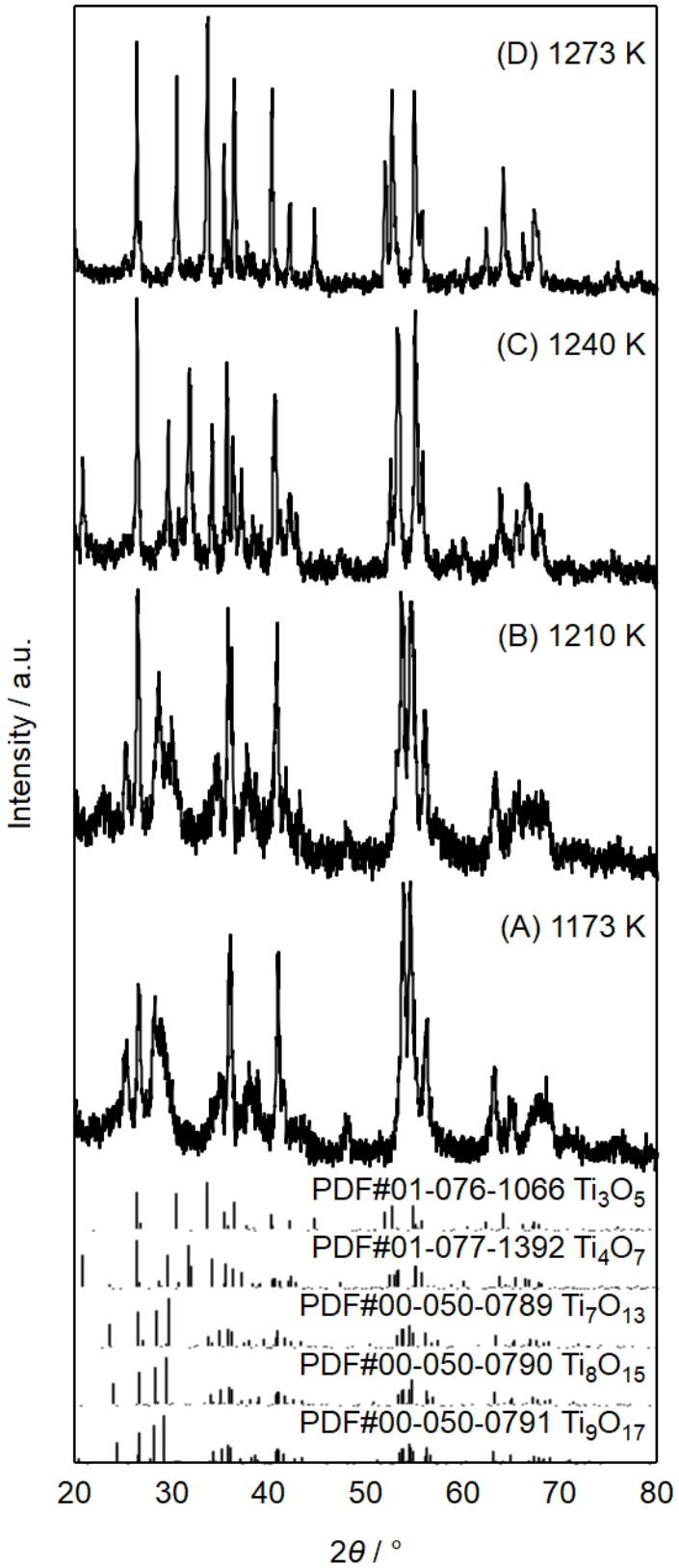

Fig. S3 X-ray diffraction (XRD) patterns of titanium suboxide supports after annealing at four different annealing temperatures, *T*: (A) 1173 K, (B) 1210 K, (C) 1240 K, and (D) 1273 K. The mass ratio of polyethylene glycol (PEG400) to titanium oxysulfate ($TiOSO_4$)-derived TiO_2 was set at 1.

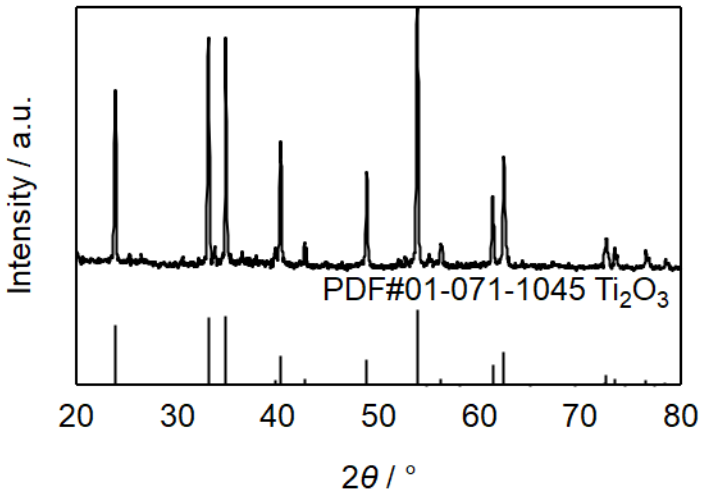

Fig. S4 XRD pattern of Ti_2O_3 particles synthesized from a mixture of TiF_4 and PEG400 at 1240 K. The mass ratio of PEG400 to TiF_4-derived TiO_2 was set at 1.

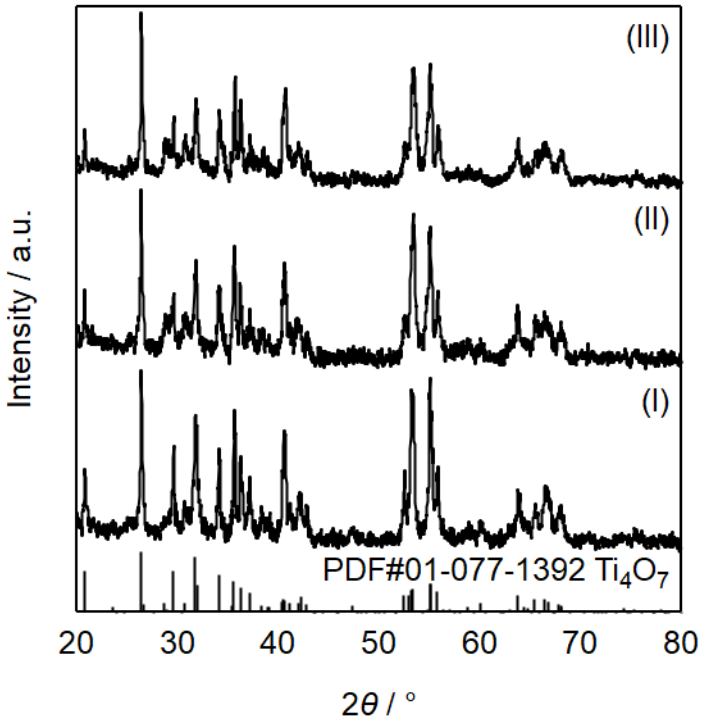

Fig. S5 XRD patterns of Ti_4O_7 particles for three different initial masses of precursor mixture in the furnace: (I) 1 g, (II) 2 g, and (III) 4 g. The mass ratio of PEG400 to $TiOSO_4$-derived TiO_2 was set at 1.

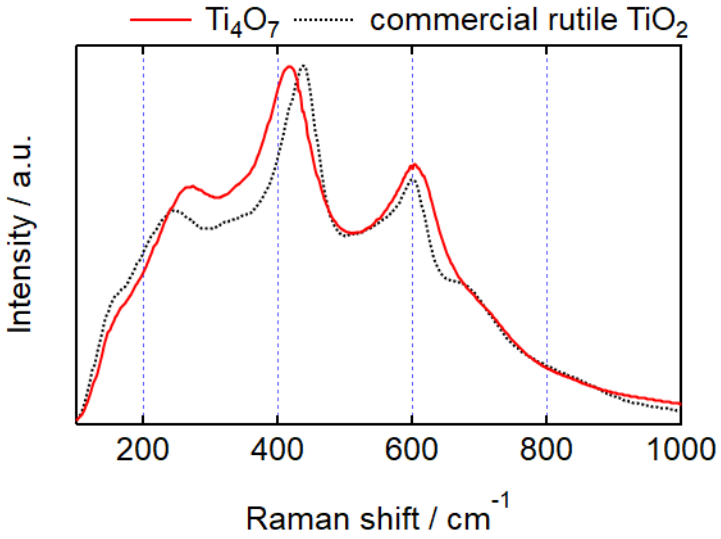

Fig. S6 Raman spectra of Ti_4O_7 synthesized from a mixture of $TiOSO_4$ and PEG400 at 1240 K and commercial rutile TiO_2 powders.

S4. The pore structure of Pt/Ti_4O_7.

The N_2 isotherm of 20% w/w Pt/Ti_4O_7 catalyst displayed in Fig. 1(d) was analyzed using the Barrett–Joyner–Halenda (BJH) method to yield the pore size distributions shown in Fig. S7. The Pt/Ti_4O_7 displays two peaks at pore diameter, *D* of approximately 4 and 5 nm which can be originated from the surface pores of Ti_4O_7, whose median size was 216.3 ± 3.4 nm. Further, Pt/Ti_4O_7 displays a broad peak at *D* of approximately 280 nm which is from the space between the aggregates of Pt/Ti_4O_7 judging from the FE-SEM image of Ti_4O_7 shown in Fig. 1(a).

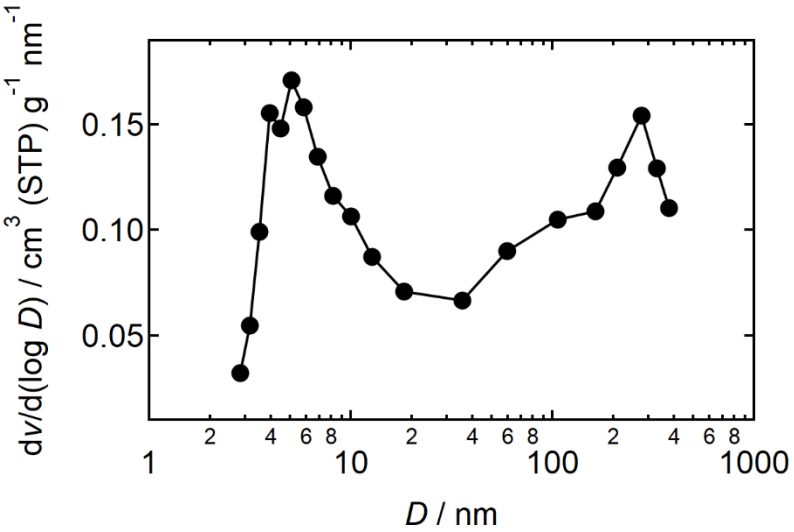

Fig. S7 A differential pore volume versus pore diameter [d*v*/d(log *D*)–*D*] curve of 20% w/w Pt/Ti_4O_7 catalyst.

S5. Chemical states of Pt/Ti_4O_7.

Effect of w_{Pt} on Pt 4f spectra of Pt/Ti_4O_7 is displayed in Fig. S8. At the lowest w_{Pt} = 5% w/w, the Pt $4f_{7/2}$ peak of Pt/Ti_4O_7 was much lower than that of commercial Pt/C, suggesting the strong metal support interactions (SMSIs) between platinum particles and Ti_4O_7 supports. The peak further shifted to lower binding energies with increasing w_{Pt}; 71.8, 71.7, 71.6 and 71.4 eV when w_{Pt} = 5, 10, 20 and 30% w/w, respectively. These results indicate that SMSI was enhanced by increasing w_{Pt}.

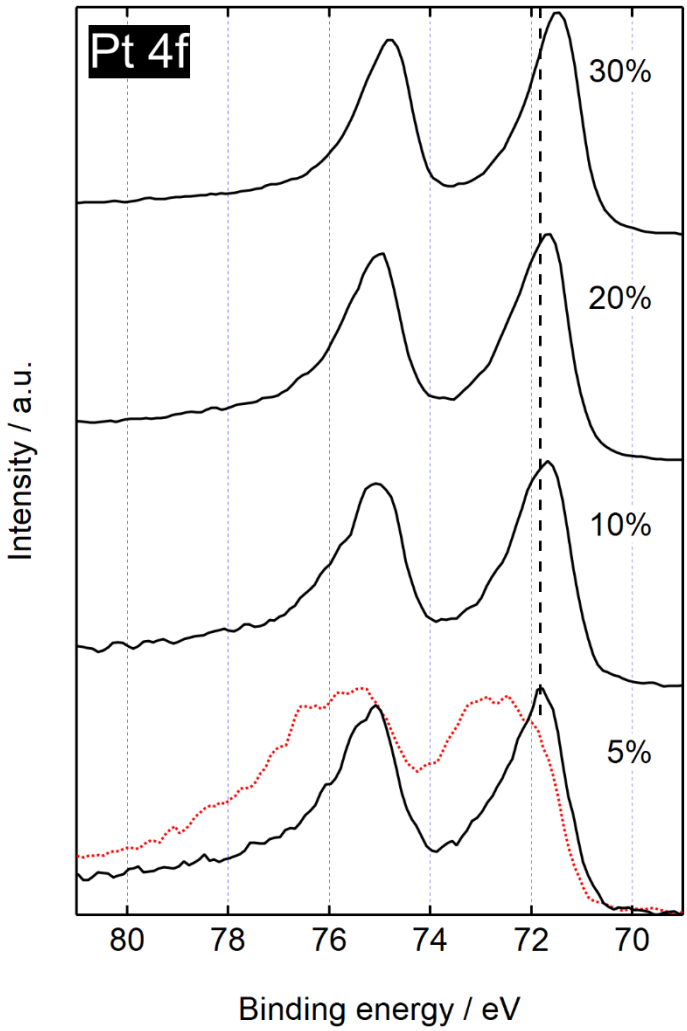

Fig. S8 Pt 4f XP spectra of Pt/Ti_4O_7 with four different w_{Pt} of 5%, 10%, 20%, and 30% w/w. For reference, a Pt 4f spectrum of commercial Pt/C catalysts is shown by the dashed curve.

S6. Crystal structure of Pt/Ti_4O_7.

Various mass fractions of platinum nanoparticles were deposited on Ti_4O_7 supports using a recently reported ethanol reduction route[S2] and their XRD patterns were collected (Fig. S9). For a w_{Pt} of 5% w/w, the XRD pattern was almost same as that before platinum deposition, as shown in Fig. S9(α) and (β), suggesting that the platinum particle size was too small to be detected by XRD, or was amorphous. Two weak broad peaks appeared at approximately 40º and 46º when w_{Pt} was 10% w/w; these were assigned to the (1 1 1) and (2 0 0) plane of the cubic platinum phases, respectively. These peaks sharpened with an increase in w_{Pt}, which was indicative of the particle growth in size. This trend was similar to that observed from carbon black-supported platinum,[S2] indicating that platinum particles were successfully deposited on the surface of Ti_4O_7, which has different properties from that of conventional carbon black.

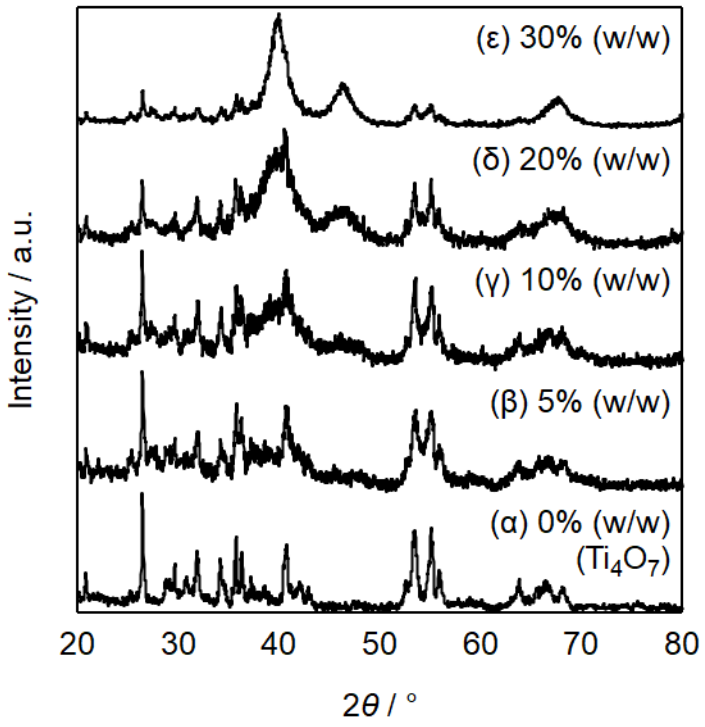

Fig. S9 XRD patterns of Pt/Ti_4O_7 for five different platinum fractions, w_{Pt}, of (α) 0% w/w, i.e., Ti_4O_7, (β) 5% w/w, (γ) 10% w/w, (δ) 20% w/w, and (ε) 30% w/w.

S7. Conductivity of Ti_4O_7.

The σ of commercial carbon black, Ketjen black EC600JD, carbothermally synthesized Ti_4O_7, and large Ti_4O_7 powders synthesized from commercial TiO_2 powders, Ti_4O_7-L, was evaluated at various pressures from 3 to 64 MPa, as shown in Fig. S10. The σ of Ti_4O_7 was high (0.7 S cm^{-1}) from the lowest P of 3 MPa, and exceeded 1 S cm^{-1} at $P \geq 6$ MPa. These values were only one order of magnitude lower than those of ECJ600JD at any P. In contrast, Ti_4O_7-L had a lower σ, particularly at low P; e.g., σ was five orders of magnitude lower than that of Ti_4O_7 at P = 3 MPa, whereas the gap was two orders of magnitude at P = 25 MPa. This differing dependence of σ on P may be a result of the difference in size shown in Fig. 1(a) and (b). As the particle size decreases, the tensile strain increased, distorting the crystal lattice to incorporate oxygen vacancies, which is known to increase the conductivity of oxides.[S10] Indeed, Ti_4O_7 particles contain a large number of oxygen vacancies on the surface, as shown by the Raman spectra (Fig. S6). Therefore, contact resistance between Ti_4O_7 particles, which is dominant for σ at low P, is suppressed owing to the high surface conductivity.

The j – V curves of MEAs fabricated using Pt/Ti_4O_7-L for four different sets of m_{Pt} at the anode and cathode are shown in Fig. S11. When the cathode m_{Pt} was increased from 0.2 to 0.5 mg_{Pt} cm^{-2}, V was significantly increased at any j, but deteriorated with further increase to 0.6 mg_{Pt} cm^{-2}, during which the anode m_{Pt} was kept at 0.2 mg_{Pt} cm^{-2}. These results indicated that the active platinum surface area was simply enlarged by increasing m_{Pt} at $\leq$ 0.5 mg_{Pt} cm^{-2}, but was decreased with a further increase of m_{Pt} to 0.6 mg_{Pt} cm^{-2}. As the particle size of Ti_4O_7-L is large (exceeding 1 μm, as shown in Fig. 1(b)), the resulting catalyst layer thickness should be larger than that of the conventional catalyst layer with Pt/C, which is typically several micrometers.[S12] Thus, ohmic loss is so large that it restricts the proton transport across the catalyst layer, and only platinum particles near the membrane side can be used for thicker layers, i.e., larger m_{Pt}. This is likely to be the main source of the decrease in V at higher m_{Pt}. When m_{Pt} was further increased to 1.0 mg cm^{-2}, V decreased at higher j, indicating increased ohmic loss at the highest catalyst layer thickness. Although the cathode m_{Pt} was optimized to 0.5 mg_{Pt} cm^{-2}, the MEA employing Pt/Ti_4O_7-L displayed a much higher ohmic loss and thus lower V when compared with

the MEA employing Pt/Ti_4O_7, as shown in Fig. 2(ii). The higher ohmic loss may have been due to the thicker catalyst layers and lower σ. The σ of Ti_4O_7-L was only 1 mS cm^{-1} for P = 10 MPa, the hot-pressing pressure of MEAs and the value is even lower than the proton conductivity of the Nafion ionomer, 0.1 S cm^{-1}.[S11] The small particle size of Ti_4O_7 enhanced the cell performance by decreasing the catalyst layer thickness and increasing σ; these changes both decreased ohmic loss, which is critical for ceramic-supported platinum catalyst layers.

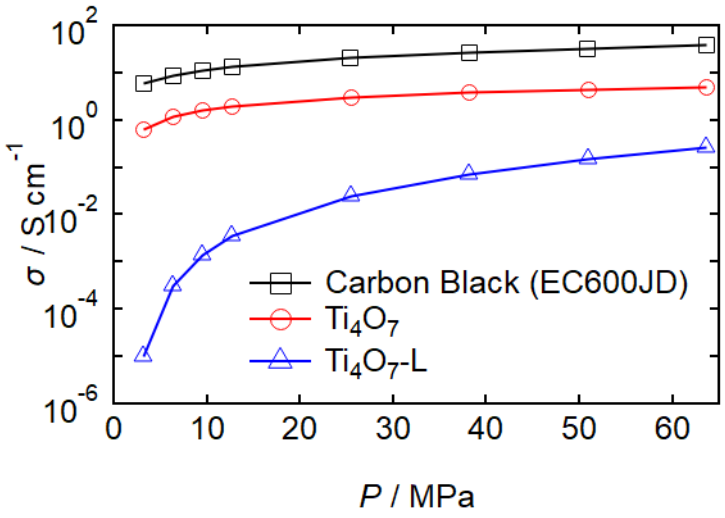

Fig. S10 Conductivity versus pressure ($\sigma - P$) curves of commercial carbon black, Ketjen black EC600JD, Ti_4O_7 particles, and large Ti_4O_7 powders synthesized from TiO_2 powders, Ti_4O_7-L.

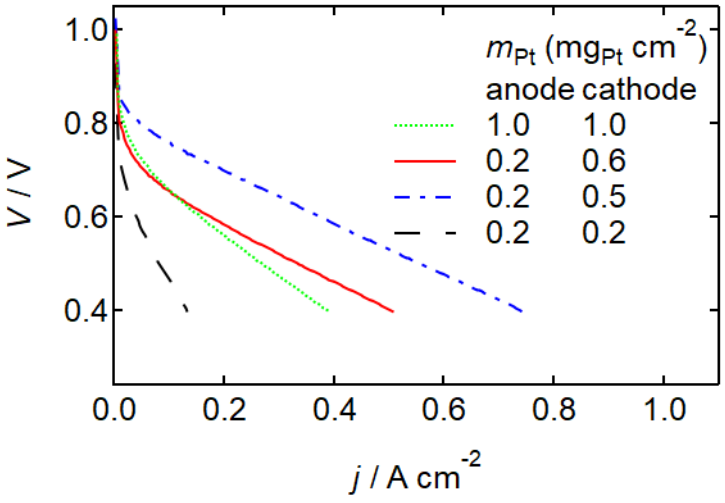

Fig. S11 $j - V$ curves of four MEAs utilizing 20% w/w Pt/Ti_4O_7-L as an anode and cathode catalyst with four different sets of anode/cathode platinum loading: m_{Pt}, at 0.2 mg_{Pt} cm^{-2}/0.2 mg_{Pt} cm^{-2}, 0.2 mg_{Pt} cm^{-2}/0.5 mg_{Pt} cm^{-2}, 0.2 mg_{Pt} cm^{-2}/0.6 mg_{Pt} cm^{-2}, and 1.0 mg_{Pt} cm^{-2}/1.0 mg_{Pt} cm^{-2}.

S8. Load cycle durability of platinum or platinum-cobalt supported on oxides.

The durability of Pt/Ti_4O_7 and Pt/SnO_2 catalysts over the 10,000 load cycles for vehicles[S4] are shown in Fig. S12. The V of an MEA employing Pt/Ti_4O_7 did not change at any j after 10,000 cycles whereas that employing Pt/SnO_2 deteriorated significantly, indicating the superior load cycle durability of Pt/Ti_4O_7 compared with Pt/SnO_2. The reported load cycle durability of platinum or platinum-cobalt catalysts supported on various oxides is summarized in Table S1. The load cycle durability of present Pt/Ti_4O_7 is among the highest of these state-of-the-art oxide-supported catalysts.

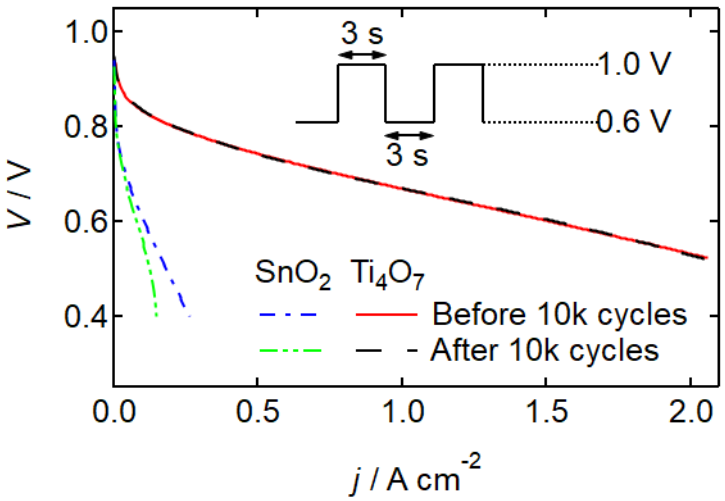

Fig. S12 $j - V$ curves of an MEA fabricated using 20% w/w Pt/Ti_4O_7 in the both anode and cathode before (solid curve) and after (dashed curve) 10,000 voltage cycles with symmetric rectangular waves (held at 0.6 V for 3 s and then at 1.0 V for 3 s). For reference, $j - V$ curves of an MEA fabricated using 20% w/w Pt/SnO_2 before (dash-dotted curve) and after (dash-double dotted curve) 10,000 cycles are also shown. The platinum loading at the anode and cathode was at 0.2 and 0.5 mg_{Pt} cm^{-2}, respectively.

Table S1 Load cycle durability of platinum or platinum-cobalt supported on various oxides evaluated in a single cell.

Cathode catalyst[*1]	w_{Pt}	m_{Pt}[*2]	Back pressure[*3]	Load cycle protocol	T_{cell}[*4]	oxidant	ΔV[*5]	Reference
Pt/Ti_4O_7	**20% w/w**	**0.5**	**Ambient pressure**	**0.6 V (3 s)–1.0 V (3s)**	**353 K**	**O_2 83%RH**	**0 mV**	**This work**
Pt/TiO_2	60.4% w/w	0.4	0.27 MPa-absolute	0.7 V (30 s)–0.9 V (30 s)	353 K	Air 100%RH	0.09 V	S13
$Pt/Ta_{0.3}Ti_{0.7}O_2$	20% w/w	0.4	Ambient pressure	0.6 V (3 s)–0.95 V (3 s)	353 K	Air 75%RH	~15 mV	S14
Pt/RuO_2-TiO_2	40% w/w	0.35	N/A	0.6 V (3 s)–0.95 V (3 s)	353 K	Air 100%RH	0.03 V	S15
Pt/IrO_2-TiO_2	8.9% w/w	0.45	0.15 MPa-absolute	0.6 V–1.0 V at 50 mV s^{-1} (triangle waves)	353 K	Air 100%RH	0.07 V	S16
						O_2 100%RH	0.07 V	
Pt/Cu,N-doped TiO_2	40% w/w	0.2	Ambient pressure	0.6 V–1.0 V at 50 mV s^{-1} (triangle waves)	348 K	O_2 100%RH	0.07 V	S17
Pt_3Co/ $Sn_{0.98}Nb_{0.02}O_2$-VGCF	N/A	0.3	N/A	0.6 V (3 s)–1.0 V (3 s)	353 K	Air 100%RH	0.09 V	S18
Pt/Nb-doped SnO_2	18.5% w/w	0.1	Ambient pressure	0.6 V (3 s)–0.94 V (60 s)	353 K	O_2 100%RH	0.08 V	S19
Pt/Sb-doped SnO_2	20% w/w	0.4	Ambient pressure	0.6 V (3 s)–0.95 V (3 s)	353 K	Air 90%RH	0.20 V	S20

[*1]Anode catalysts were commercial Pt/C except for this work, in which 20% w/w Pt/Ti_4O_7 was used for both the anode and cathode

[*2]Cathode platinum loading in mg_{Pt} cm^{-2}

[*3]Cathode back pressure

[*4]Cell temperature

[*5]Decrease in V after 10,000 cycles (except for references S13, S18, and S20, which used 5,000 cycles). References S16 and S19 report the decrease in $V + IR$ after 10,000 cycles.

Supplementary references

S1 Q. Pang, D. Kundu, M. Cuisinier and L. F. Nazar, *Nat. Commun.*, 2014, **5**, 4759.

S2 Md. M. Rahman, K. Inaba, G. Batnyagt, M. Saikawa, Y. Kato, R. Awata, B. Delgertsetsega, Y. Kaneta, K. Higashide, T. Uruga, Y. Iwasawa, K. Ui and T. Takeguchi, *RSC Adv.*, 2021, **11**, 20601.

S3 T. Vidaković, M. Christov and K. Sundmacher, *Electrochim. Acta*, 2007, **52**, 5606.

S4 A. Ohma, K. Shinohara, A. Iiyama, T. Yoshida and A. Daimaru, *ECS Trans.*, 2011, **41**, 775.

S5 J. R. Smith, R. L. Clarke and F. C. Walsh, *J. Appl. Electrochem.*, 1998, **28**, 1021.

S6 U. Balachandran and N.G. Eror, *J. Solid State Chem.*, 1982, **42**, 276.

S7 P. J. Huang, H. Chang, C. T. Yeh and C. W. Tsai, *Thermochim. Acta*, 1997, **297**, 85.

S8 J. C. Parker and R. W. Siegel, *Appl. Phys. Lett.*, 1990, **57**, 943; X. H. Wang, J. G. Li, H. Kamiyama, M. Katada, N. Ohashi, Y. Moriyoshi and T. Ishigaki, *J. Am. Chem. Soc.*, 2005, **127**, 10982.

S9 Y. Du, Z. Dohnálek and I. Lyubinetsky, *J. Phys. Chem. C*, 2008, **112**, 2649.

S10 M. Zhang, Y. Wang, Y. Zhang, J. Song, Y. Si, J. Yan, C. Ma, Y. T. Liu, J. Yu and B. Ding, *Angew. Chem. Int. Ed.*, 2020, **59**, 23252.

S11 Y. Sone, P. Ekdunge and D. Simonsson, *J. Electrochem. Soc.*, 1996, **143**, 1254.

S12 M. Chisaka and H. Daiguji, *J. Electrochem. Soc.*, 2009, **156**, B22.

S13 S. Y. Huang, P. Ganesan and B. N. Popov, *Appl. Catal. B*, 2011, **102**, 71.

S14 A. Kumar and V. Ramani, *ACS Catal.*, 2014, **4**, 1516.

S15 J. Parrondo, T. Han, E. Niangar, C. Wang, N. Dale, K. Adjemian and V. Ramani, *Proc. Natl Acad. Sci.*, 2014, **111**, 45.

S16 A. Pătrua, A. Rabis, S. E. Temmel, R. Kotz and T. J. Schmidt, *Catal. Today*, 2016, **262**, 161.

S17 P. Dhanasekaran, S. V. Selvaganesh and S. D. Bhat, *New J. Chem.*, 2017, **41**, 13012.

S18 S. Matsumoto, M. Nagamine, Z. Noda, J. Matsuda, S. M. Lyth, A. Hayashi and K. Sasaki, *J. Electrochem. Soc.*, 2018, **165**, F1164.

S19 C. Takei, R. Kobayashi, Y. Mizushita, Y. Hiramitsu, K. Kakinuma and M. Uchida, *J. Electrochem. Soc.*, 2018, **165**, F1300.

S20 C. He, X. Wang, S. Sankarasubramanian, A. Yadav, K. Bhattacharyya, X. Liang and V. Ramani, *ACS Appl. Energy Mater.*, 2020, **3**, 5774.